An Air–Sea Interaction Model of Intraseasonal Oscillations in the Tropics

KERRY A. EMANUEL

Center for Meteorology and Physical Oceanography, Massachusetts Institute of Technology, Cambridge, MA 02139

(Manuscript received 30 July 1986, in final form 27 February 1987)

ABSTRACT

We present a linear model of intraseasonal oscillations produced by the interaction of an atmosphere on an equatorial Beta-plane with a fixed ocean. Convection is treated as a means of rapidly redistributing in the vertical heat acquired from the sea surface, rather than as a heat source in and of itself. The model produces a spectrum of equatorially trapped oscillating instabilities, among which is an eastward-propagating wavenumber 1 disturbance with an intrinsic phase speed in the range of 4–20 m s^{-1}, depending on the mean zonal wind, the surface exchange coefficients, the air–sea equivalent potential temperature difference, and the difference of absolute temperature across the depth of the lower troposphere. The three-dimensional structure of this mode is in excellent agreement with observations and recent numerical experiments concerning the 30–60 day oscillation. The phase speed and growth rate of the disturbances depend only on conditions at the equator, while their meridional structure varies with meridional gradients of mean zonal wind, sea surface temperature, and the depth of the moist convective layer. Momentum fluxes by the waves may serve to maintain mean easterlies at the equator. The model also predicts nongeostrophic oscillations with generally shorter periods of around one week.

1. Introduction

Observations of the tropical atmosphere have revealed two prominent low-frequency modes of oscillation which have received increasing attention in recent years. These are the El Niño–Southern Oscillation (ENSO), which occurs over a period of about a year, and the 30–60 day oscillation discovered by Madden and Julian (1971, 1972). Possible links between these two phenomena have been discussed by Lau and Chan (1985, 1986), among others. While ENSO has been extensively documented and studied from a theoretical perspective (e.g., Cane, 1983; McCreary and Anderson, 1984), the fundamental cause of the 30–60 day oscillation has not been as widely addressed and remains a mystery. This paper attempts a simple explanation of the phenomenon.

The 30–60 day oscillation was first detected in time series of zonal wind at Canton Island in the Pacific by Madden and Julian (1971), who found that the strongest signals, at 850 and 150 mb, were nearly out of phase, suggesting that the phenomenon is essentially baroclinic. The oscillation has also been detected in the total atmospheric relative angular momentum (Langely et al., 1981; Anderson and Rosen, 1983; Rosen and Salstein, 1983), outgoing longwave radiation (Weickmann, 1983; Lau and Chan, 1983a,b; 1985; 1986; Weickmann et al., 1985) and divergent circulation (Lorenc, 1984; Krishnamurti et al., 1985). The oscillation appears to be confined to within 30° latitude of the equator (Madden and Julian, 1972) and to represent a wavenumber 1 disturbance propagating eastward at about 10 m s^{-1}. Madden and Julian (1972), Krishnamurti et al. (1985) and Anderson and Rosen (1983) also find evidence of poleward phase propagation. Parker (1973) has shown evidence that the eastward phase propagation of zonal winds is confined to the longitude range of about 100°E to the dateline, although Krishnamurti et al. (1985) show a wave in the 200 mb velocity potential which travels the full distance around the world. This apparent contradiction may be resolved by recent observations reported by Lau and Chan (1986), which show considerable interannual variability in the eastward extent of phase propagation of outgoing longwave radiation anomalies.

Of considerable interest in understanding the underlying cause of the 30–60 day oscillation is a recent paper of Hayashi and Sumi (1986), who used a general circulation model with an ocean-covered earth to study the oscillation. They found a prominent 30 day eastward-propagating wave within about 10° of the equator. The structure of the wave is in good agreement with observations of the 30–60 day oscillation, showing a 180° phase shift of zonal wind perturbation over the depth of the troposphere and a temperature wave which is nearly (but not quite) in phase with the upper tropospheric zonal wind perturbation. To the extent that this feature is a model analog of the observed 30–60 day wave, we may infer that neither land–sea contrasts nor zonal asymmetry is necessary to explain the basic mechanism of the oscillation.

There have been few theoretical investigations of the

30–60 day oscillation. Parker (1973) originally proposed that the phenomenon represents an equatorially trapped Kelvin wave, but the observed vertical wavelength yields phase speeds of 30–60 m s^{-1}: far too large to explain the observed wave. Chang (1977) showed that the introduction of dissipation and Newtonian cooling could effect a reduced phase speed, but as pointed out by Stevens and White (1979), the resulting phase speed is very dependent on the damping coefficients. Webster (1983) showed that a proper treatment of the oceanic and continental hydrological cycle could yield a wave of the observed period in simulations of air motions over the Indian ocean. The northward progression of the signal in the simulation is attributed to the temperature contrast between the Indian subcontinent and the adjacent ocean. While this may have some bearing on the observed phenomenon, it does not explain its global scale or the 30 day wave in Hayashi and Sumi's experiment. Goswami and Shukla (1984) found symmetric intraseasonal oscillation modes of Hadley cells, but these lack the dominant wavenumber 1 structure of the observed and numerically modeled circulations. Finally, wave-CISK models (e.g., Hayashi, 1970; Lindzen, 1974) lead to waves whose structure and phase speed strongly match those of free Kelvin modes and are thus not satisfactory models of the observed waves.

In view of these difficulties, we here propose a new model of the 30–60 day wave which is driven by the interaction of the atmosphere with a fixed ocean.[1] Unlike conditional instability of the second kind (CISK), which regards convection as a means of releasing stored potential energy, we view convection as a way of rapidly distributing through the depth of the troposphere heat acquired from the sea surface. A conceptual picture of the wave on the equator is illustrated in Fig. 1. If the mean surface wind is from the east, it follows that perturbation easterlies will result in an anomalously large flux of latent (and possibly sensible) heat from the sea surface, since the planetary boundary layer is undersaturated with respect to the ocean. Conversely, perturbation westerlies will be associated with negative anomalies of surface heat flux. If convection distributes the heat anomalies through the depth of the troposphere, then the tropospheric heating will lead the wave vertical velocity by a quarter wavelength, so that the phase propagation is eastward. Since the temperature anomalies will have a component which is in-phase with vertical velocity, potential energy is converted to mechanical energy which can lead to the growth of the wave or, in the mature stage, can supply the energy necessary to overcome dissipation.

In the remainder of this paper we attempt to quantify this conceptual notion of the mechanism of the 30–60 day oscillation and to determine its meridional structure. We will show that a linear model of this mechanism also predicts faster, nongeostrophic oscillations. In the following section, we derive a simple representation of the effect of surface heat fluxes and the subsequent vertical redistribution of the heat on the surface pressure. The basic linear model is derived and solved in section 3. In section 4 we discuss possible scale-selection mechanisms. Subsequent sections examine the effects of meridionally and zonally varying sea surface temperature and zonal wind on the unstable modes.

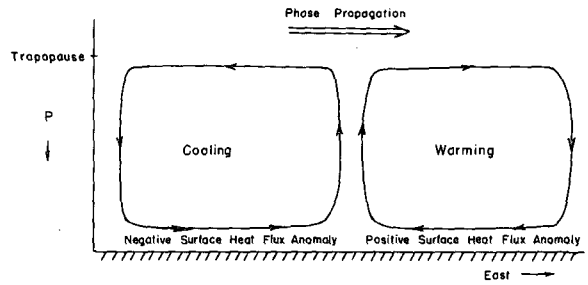

FIG. 1. Conceptual illustration of the 30–60 day wave as an air–sea interaction instability. Anomalously strong easterlies at right give rise to anomalous heat fluxes from the sea surface; the moist entropy is then rapidly redistributed aloft by convection. The resulting temperature anomaly leads the surface convergence by one quarter cycle, leading to wave growth and eastward propagation.

2. Treatment of convection

For the present purpose, we wish to devise a simple, qualitatively correct representation of the vertical redistribution of heat by convection. Accordingly, we make two assumptions. The first is that *the temperature structure of the troposphere above the subcloud layer is maintained at the moist adiabatic lapse rate, with the particular value of the saturation moist entropy determined by the boundary layer moist entropy.* This may be expressed symbolically

$$s^* = s_b, \tag{1}$$

where s^* is the saturation moist entropy of the troposphere above the subcloud layer and s_b is the subcloud layer moist entropy. Betts (1982) has shown that the tropics are more nearly characterized by a *virtual* moist adiabatic lapse rate, which is defined to include the effects of condensate loading, but we use (1) here for simplicity.[2]

The second assumption is that *fluctuations in the boundary layer moist entropy are linearly proportional to fluctuations in the pressure-weighted mean of moist entropy through the depth of the troposphere:*

[1] Since the original submission of this paper the author has learned of a similar idea by Neelin et al. (1987).

[2] By assuming this simple vertical distribution of temperature fluctuations, we limit the vertical structure of the model's modes to troposphere-deep baroclinic waves.

$$\delta s_b = \nu \delta \bar{s}, \tag{2}$$

where ν is the proportionality constant and $\delta\bar{s}$ is the fluctuating component of pressure-weighted mean moist entropy. Combining this with (1) yields a relationship between fluctuations in the (constant) saturation moist entropy and fluctuations in the mean moist entropy of the troposphere:

$$\delta s^* = \nu \delta \bar{s}.$$

In the Appendix we show that ν may be related to the percentage of surface evaporation anomalies realized as precipitation or, alternatively, to fluctuations of tropospheric relative humidity. In precipitating regions ν is close to unity, otherwise it may be very small. We assume here that the waves occur in precipitating regions of the atmosphere.

Note that, according to (1), no matter how much or how little "moisture convergence" occurs, no temperature changes will result in the free atmosphere unless the moist entropy of the boundary layer changes; this implies that adiabatic cooling exactly cancels condensation heating when there is moisture convergence at uniform θ_e. This points to the defect of most simple representations of convection in linear CISK models; namely, that small errors in the closure on the heating itself are likely to produce very large errors in the small difference between heating and adiabatic cooling.[3]

As a final step, we relate fluctuations in the geopotential height field to fluctuations in s^* using the hydrostatic relation, which may be written

$$\frac{\partial \phi}{\partial p} = -\alpha,$$

where ϕ is the geopotential and α is the specific volume. If we divide ϕ and α into mean and fluctuating components at each pressure level, it follows that

$$\frac{\partial \delta\phi}{\partial p} = -\delta\alpha, \tag{3}$$

where $\delta\phi$ and $\delta\alpha$ are the fluctuating components of ϕ and α. Now through the equation of state we can relate α to any other two state variables, which we choose to be p and s^*. Thus

$$(\delta\alpha)_p = \left(\frac{\partial \alpha}{\partial s^*}\right)_p \delta s^*. \tag{4}$$

A fundamental relationship from the first law of thermodynamics (see Emanuel, 1986, appendix A) is

$$\left(\frac{\partial \alpha}{\partial s^*}\right)_p = \left(\frac{\partial T}{\partial p}\right)_{s^*}.$$

Combining this relation with (4) and using (2), (3) may be written

$$\frac{\partial \delta\phi}{\partial p} = -\left(\frac{\partial T}{\partial p}\right)_{s^*} \delta s_b. \tag{5}$$

The above may be directly integrated to yield

$$\delta\phi - \delta\phi_b = (T_b - T)\delta s_b. \tag{6}$$

In general, fluctuations in the geopotential field can be divided into barotropic and baroclinic components corresponding to barotropic and baroclinic components of the horizontal wind. As we shall be dealing with a barotropically stable basic state, the linearly unstable modes must be strictly baroclinic so that in a system bounded above and below by surfaces along which $dp/dt = 0$, the vertically integrated mass-weighted horizontal velocity fluctuations must vanish. Through the equations of motion, this implies that the fluctuating components of the horizontal pressure gradient acceleration, integrated in pressure through the domain, must also vanish. From (6), then, we have

$$\frac{1}{\Delta p}\int_{p_t}^{1000} \delta\phi = \delta\phi_b + \delta s_b\left[T_b - \frac{1}{\Delta p}\int_{p_t}^{1000} T dp\right] = 0, \tag{7}$$

where p_t is the tropopause pressure and $\Delta p = 1000 - p_t$. From (7) it follows that

$$\delta\phi_b = -\delta s_b[T_b - \bar{T}], \tag{8}$$

where $\bar{T}$ is the pressure-weighted mean absolute temperature:

$$\bar{T} \equiv \frac{1}{\Delta p}\int_{p_t}^{1000} T dp.$$

Using the relation $s = C_p \ln\theta_e$, where C_p is the heat capacity at constant pressure and θ_e is the equivalent potential temperature, and using (2), we rewrite (8) as

$$\delta\phi_b = -C_p T_b \epsilon \nu \delta \ln\bar{\theta}_e, \tag{9}$$

where ϵ may be regarded as the thermodynamic efficiency:

$$\epsilon \equiv \frac{T_b - \bar{T}}{T_b}. \tag{10}$$

Thus, our final closure for purely baroclinic modes in the tropics relates fluctuations in surface pressure to fluctuations in tropospheric mean θ_e, with the proportionality constant related to a mean thermodynamic efficiency and to the percentage of surface evaporation anomaly realized as precipitation.

3. The basic model

The simple representation of moist convection discussed in the previous section relates the geopotential at the top of the boundary layer to tropospheric mean

[3] It should be noted that fully nonlinear implementations of moisture convergence-based closure schemes such as that of Kuo (1974) may produce the same result as (2) after an initial period of adjustment. This is because moisture convergence will rapidly adjust the initial subadiabatic temperature back to adiabatic; thereafter, temperature changes for sufficiently slow large scale fluctuations will follow the temperature changes of parcels lifted adiabatically from the boundary layer.

θ_e. Under the further very mild assumption that fluctuations of geopotential in the boundary layer are independent of height, this allows a determination of the horizontal velocity at the top of the surface layer using only the equations of motion evaluated there and an equation governing $\bar{\theta}_e$. The horizontal equations of motion on an equatorial β plane may be written

$$\frac{du}{dt} = -\frac{\partial \phi}{\partial x} + \beta y v - g\frac{\partial \tau_x}{\partial p} + E, \tag{11}$$

$$\frac{dv}{dt} = -\frac{\partial \phi}{\partial y} - \beta y u - g\frac{\partial \tau_y}{\partial p}, \tag{12}$$

where the symbols have their usual meanings and τ_x and τ_y are the stresses. E is an ad hoc eddy stress term which is necessary to sustain a mean zonal wind at the equator, as will be demonstrated presently.

We postulate a zonally and vertically constant mean easterly wind in the vicinity of the equator. This neglects the meridional flow associated with the Hadley circulation, but this will be small sufficiently close to the equator. According to (11) and (12), then,

$$g\frac{\partial [\tau]_x}{\partial p} = [E], \tag{13}$$

$$\frac{\partial [\phi]}{\partial y} = -\beta y [U], \tag{14}$$

where the brackets denote time averages.

In (14) we have neglected the meridional stress term under the plausible assumption that it is a function of the meridional wind. According to these relations, the frictional stress in the zonal direction is balanced by a horizontal eddy flux of momentum, while the zonal flow itself is in geostrophic balance.

A major problem that occurs in this analysis is the determination of the vertical derivative of the turbulent stresses within the boundary layer. Both observations and numerical models (e.g., Hayashi and Sumi, 1986) show that the velocity amplitudes of 30–50 day oscillations have peaks near 850 mb rather than near the ground, implying substantial vertical variation of the divergence of the turbulent stresses across the top of the boundary layer. Calculations by Deardorff (1972) for the unstable planetary boundary layer show that the stresses decrease nearly linearly between the surface and the top of the boundary layer, though in that case there was no cumulus convection. It is not clear how efficient cumulus clouds might be in carrying the turbulent stresses beyond the top of the subcloud layer. In view of these difficulties, we here assume that the turbulent stress varies linearly between the surface and some pressure level p_m which is at or perhaps above the top of the subcloud layer:

$$\frac{\partial \tau}{\partial p} = \frac{1}{\Delta p_m}\tau_a = \frac{\rho_a}{\Delta p_m} C_D |\mathbf{V}_a| \mathbf{V}_a, \tag{15}$$

where Δp_m is the difference between surface pressure and p_m, ρ_a is the density and $\mathbf{V}_a$ is the vector horizontal wind. The subscript a denotes evaluation at the top of the surface layer. We have used the standard bulk aerodynamic relation for the stress in the surface layer, with exchange coefficient C_D. We now linearize (11) and (12) about the mean state given by (13) and (14), using (15) for the stresses. The results are

$$\frac{\partial u}{\partial t} + [U]\frac{\partial u}{\partial x} = -\frac{\partial \phi}{\partial x} + \beta y v - 2\frac{C_D}{h}|[U]|u + E, \tag{16}$$

$$\frac{\partial v}{\partial t} + [U]\frac{\partial v}{\partial x} = -\frac{\partial \phi}{\partial y} - \beta y u - \frac{C_D}{h}|[U]|v, \tag{17}$$

where the variables without brackets are the perturbation quantities evaluated at the top of the surface layer, and h is a boundary layer scale height defined

$$h \equiv \frac{\Delta p_m}{p_a}\frac{RT_a}{g}. \tag{18}$$

This has been derived using the ideal gas law for ρ_a in (15). For lack of knowledge of the perturbation horizontal eddy stress E we henceforth neglect it.

The thermodynamic equation may be written

$$\frac{d \ln\theta_e}{dt} = -g\frac{\partial \tau_{\theta_e}}{\partial p} + \dot{R}, \tag{19}$$

where τ_{θ_e} is the vertical eddy flux of $\ln\theta_e$ and $\dot{R}$ is the radiative cooling. The radiative convective equilibrium of the mean state is expressed by

$$g\frac{\partial [\tau]_{\theta_e}}{\partial p} = [\dot{R}].$$

Linearizing (19) about this mean state yields

$$\frac{\partial \ln\theta_e}{\partial t} + [U]\frac{\partial \ln\theta_e}{\partial x} = -g\frac{\partial \tau_{\theta_e}}{\partial p} + \dot{R}, \tag{20}$$

where the variables without brackets now represent the perturbations. To derive an equation for $\bar{\theta}_e$, (20) may be integrated from the top of the surface layer to the tropopause to yield

$$\frac{\partial \ln\bar{\theta}_e}{\partial t} + [U]\frac{\partial \ln\bar{\theta}_e}{\partial x} = -\frac{g}{\Delta p}\tau_{\theta_{ea}} + \frac{1}{\Delta p}\int_{p_t}^{p_a} \dot{R}dp. \tag{21}$$

If the total flux of $\ln\theta_e$ at the top of the surface layer is governed by a bulk aerodynamic formulation of the form

$$\tau_{\theta_{ea}} + [\tau_{\theta_{ea}}] = \rho_a C_\theta |V|(\ln\theta_e - \ln\theta_{es}),$$

where θ_{es} is the saturation θ_e of the sea surface, the linearization of the above gives

$$\tau_{\theta_{ea}} = [\rho_a]C_\theta|[U]|\ln\theta_e - [\rho_a]C_\theta \operatorname{sgn}([U])\left[\ln\frac{\theta_{es}}{\theta_e}\right]u, \tag{22}$$

where we have neglected fluctuations in ρ_a. Finally, we assume that the perturbation radiative cooling given

by this last term in (21) can be represented as a Newtonian cooling:

$$\frac{1}{\Delta p}\int_{p_t}^{p_b}\dot{R}dp = -\tau_{\text{rad}}^{-1}\ln\overline{\theta_e}, \tag{23}$$

where τ_{rad} is a radiative time scale for vertically integrated θ_e (or θ_e^*). Incorporating (23) and (22) in (21) and using (2), there results

$$\frac{\partial \ln\overline{\theta_e}}{\partial t}+[U]\frac{\partial \ln\overline{\theta_e}}{\partial x} = -\frac{C_\theta}{H}\nu[U]\ln\bar{\theta}_e + \frac{C_\theta}{H}\left[\ln\frac{\theta_{es}}{\theta_e}\right]\text{sgn}([U])u - \tau_{\text{rad}}^{-1}\ln\overline{\theta_e}, \tag{24}$$

where

$$H=\frac{\Delta p}{p_a}\frac{RT_a}{g}.$$

The system comprised of (16) (neglecting E), (17), (24) and (9) represents a closed set of linear equations with constant coefficients. To simplify the expressions, we nondimensionalize all variables (with some hindsight) according to

$$\begin{aligned} x^* &= ax,\\ y^* &= A^{1/4}\beta^{-1/2}a^{1/4}y,\\ t^* &= a^{1/2}A^{-1/2}t,\\ u^* &= A^{1/2}a^{1/2}u,\\ v^* &= A^{3/4}\beta^{-1/2}a^{-1/4}v,\\ \ln\theta_e^* &= aH^{-1}C_\theta\left[\ln\frac{\theta_{es}}{\theta_e}\right]T,\\ [U]^* &= A^{1/2}a^{1/2}U, \end{aligned} \tag{25}$$

where the asterisks denote the dimensional variables, and the constants are defined

$$\left.\begin{aligned} &a \equiv \text{radius of earth}\\ &\beta \equiv \text{meridional gradient of Coriolis parameter}\\ &A \equiv \epsilon\nu C_p T_a H^{-1} C_\theta[\ln\theta_{es}/\theta_e] \end{aligned}\right\}. \tag{26}$$

We shall seek normal mode solutions of the form

$$e^{ikx+\sigma t},$$

with σ the complex growth rate.

With these substitutions, (16), (17) and (24) may be written

$$(D+2F)u = ikT + yv, \tag{27}$$

$$(D+F)v = P\left[\frac{dT}{dy} - yu\right], \tag{28}$$

$$(D+\gamma)T = u\,\text{sgn}([U]), \tag{29}$$

where $D \equiv \sigma + ik[U]$, and the dimensionless constants are defined

$$\begin{aligned} F &\equiv C_D|[U]|a^{1/2}A^{-1/2}h^{-1},\\ P &\equiv \beta A^{-1/2}a^{3/2},\\ \gamma &\equiv a^{1/2}A^{-1/2}\tau_{\text{rad}}^{-1} + F\nu\frac{C_\theta}{C_D}\frac{h}{H}. \end{aligned}$$

The relation (9) has been used in place of ϕ in (16) and (17). The system comprised of (27)–(29) is very similar to one considered by Neelin et al. (1987), although the latter included a moist stratification term in the temperature equation (29).

We note immediately that at the equator, where $y = 0$, (28) is uncoupled with (27) and (29), provided u and T are finite at $y = 0$. Then (27) and (29) may immediately be combined to yield the dispersion relation

$$(D+2F)(D+\gamma) = ik\,\text{sgn}([U]). \tag{30}$$

Inspection of (27)–(29) shows that in this case $v = 0$ everywhere, so that the meridional structure is obtained through

$$\frac{dT}{dy} = yu = y(D+\gamma)\,\text{sgn}([U])T,$$

the solution of which is

$$T = B\exp\left[\frac{1}{2}y^2(D+\gamma)\,\text{sgn}([U])\right], \tag{31}$$

where B is a constant. It is seen immediately that *for growing waves (*$\text{Re}(D) > 0$*), well-behaved solutions are only possible when* $[U] < 0$. We shall henceforth deal strictly with easterly mean winds.

Estimates of the thermal damping coefficient γ reveal that it is at least an order of magnitude less than F as long as the Reynolds stresses decrease to zero over a scale not much larger than the depth of the subcloud layer. We therefore neglect γ in (30) and, as mentioned before, take $[U] < 0$. The solutions for the real and imaginary parts of D are then

$$\begin{aligned} D_r &= \left\{\frac{1}{2}[F^2 + (F^4+k^2)^{1/2}]\right\}^{1/2} - F\\ D_i &= -\frac{k}{2}\left\{\frac{1}{2}[F^2 + (F^4+k^2)^{1/2}]\right\}^{-1/2}. \end{aligned} \tag{32}$$

This shows that the intrinsic phase speed is always positive and that the growth rate increases with wavenumber. In the limit of large friction F ($k \ll F^2$) the growth rate and phase speed are:

$$\begin{aligned} F^2 &\overset{\text{Lim}}{\gg} k^{\sigma_r = 1/8k^2/F^3}\\ F^2 &\overset{\text{Lim}}{\gg} k^{c=1/2F^{-1}+U}, \end{aligned} \tag{33}$$

showing that in this case the phase speed (c) is independent of wavenumber. In the limit of large k, on the other hand, (32) shows that $\sigma_r \approx k^{1/2}$ and $c \approx k^{-1/2}$. The linear theory does not select the longest waves; reasons for this disparity will be discussed in section 4.

Since F is linearly proportional to $[U]$ the growth rates and phase speeds are sensitive to the mean zonal wind. Table 1 lists dimensional values of the (ground-relative) phase speeds and growth rates as functions of the mean zonal wind and wavenumber. The dimensional parameters used to calculate these are listed at the bottom of the Table. The sea–air θ_e difference represents 78% relative humidity at a temperature of 27°C and Jordan's (1958) hurricane season sounding has been used to estimate ϵ. The surface exchange coefficients have been estimated from Deardorff (1972) under neutral conditions. The most problematic estimate is that of h which controls the depth over which the boundary layer Reynolds stresses decrease to zero. If we assume, in the extreme limit, that the cumulus momentum fluxes are so efficient as to distribute the stresses linearly through the troposphere then F will be much smaller than the other terms in (32) so that $\sigma_r \approx (k/2)^{1/2}$ and $c \approx (1/2k)^{1/2}$. For parameter values listed in Table 1 this gives wavenumber 1 growth rates of about 0.27 day^{-1} and periods of about 23 days.

The phase speeds are sensitive to $[U]$ but do not vary rapidly with wavenumber. Wavenumber 1 periods of 30–60 days obtain when $-[U]$ is between about 1 and 3 m s^{-1}. The dominant effect of the mean wind is not the Doppler shifting but rather in the control of the friction coefficient F. Thus the mean surface wind is crucial in determining the phase speeds. Mean equatorial surface winds from Newell et al. (1972) lie generally in this range.

Since the phase speeds do vary somewhat with surface conditions, thermodynamic efficiency, and the pressure depth of the troposphere, one might expect the phase speed and amplitude to be modulated as the wave travels around the world. In particular, the largest amplitudes and phase speeds will occur over the warmest water, where $\ln\theta_{es}/\theta_e$ and ϵ are large. Diagrams of phase propagation of outgoing longwave radiation anomalies in Lau and Chan (1986) and Murakami et al. (1986) clearly show the diminishment of both phase speed and amplitude as the waves cross toward colder water in the region near the date line.

TABLE 1. Dimensional growth rates, ground-relative phase speeds and periods as functions of U^* and Wavenumber k†.

k	$-U^*$ (m s^{-1})	σ_r (day^{-1})	c^* (m s^{-1})	Period (days)
1	4	0.01	3.7	127
	3	0.02	7.2	64
	2	0.05	11.9	39
	1	0.13	17.1	27
2	4	0.03	3.7	64
	3	0.06	6.4	36
	2	0.12	9.6	24
	1	0.23	12.6	18
3	4	0.06	3.4	45
	3	0.11	5.8	27
	2	0.19	8.2	19
	1	0.31	10.1	15

† The following values are assumed:

$[\ln\theta_{es}/\theta_e] = 0.035$ $\quad C_\theta = 1.2\times10^{-3}$
$\epsilon = 0.1$ $\quad H = 8$ km
$\nu = 0.8$ $\quad h = 500$ m
$C_D = 1\times10^{-3}$ $\quad a = 6.38\times10^3$ km

Figure 2 shows the horizontal structure of wavenumber 1 for the case that $F = 0.9$ and $\gamma = 0.2$, deduced from (31) and (29). Also shown are the vertical velocity and an estimate of the cumulus mass flux. The former is calculated from mass continuity, i.e.,

$$w = -iku,$$

where w has been normalized according to

$$w^* = h' A^{1/2} a^{-1/2} w,$$

where h' is half the depth of the wave. The estimate of the cumulus mass flux is made using the relationship

$$w^* = M_c^* + M_d^*, \tag{34}$$

where M_c^* and M_d^* are the cloud and environmental fractional mass fluxes. The environmental mass flux is estimated by requiring the subsidence outside the clouds to account for the temperature changes in the wave. That is, we require that in the middle troposphere,

$$\frac{\partial \ln\theta}{\partial t} + [U]\frac{\partial \ln\theta}{\partial x} = -M_d^* \frac{N^2}{g}, \tag{35}$$

where N is the buoyancy frequency (for dry air) and θ is the potential temperature. From thermodynamic considerations, it may be shown that

$$d\ln\theta|_p = \frac{\Gamma_m}{\Gamma_d} d\ln\theta_e^*|_p,$$

where Γ_m and Γ_d are the moist and dry adiabatic lapse rates, respectively. Using this together with the same normalization for M_d as used for w, and the normalization of $\ln\theta_e^*$ given by (25), we get

$$M_d = -G(DT), \tag{36}$$

with $D = \sigma + ik[U]$ and $G \equiv gav(\Gamma_m/\Gamma_d) \times h^{-1}N^{-2}H^{-1}C_\theta[\ln\theta_{es}/\theta_e]$. For the values of the parameters listed in Table 1, $\Gamma_m/\Gamma_d = 0.6$, $h' = 5$ km, and $N^2 = 10^{-4}$ s^{-2} $G = 0.19$. Using (36), the dimensionless form of (34) may be written

$$M_c = w + G(DT). \tag{37}$$

Since $G \approx 0.2$, most of the cumulus flux is due to forced ascent in the wave, with the remainder due to surface latent heating. This is another way of saying that the great majority of latent heat release in clouds is due to moisture convergence, with the rest coming from evaporation. In our theory, the part due to moisture convergence alone exactly balances adiabatic

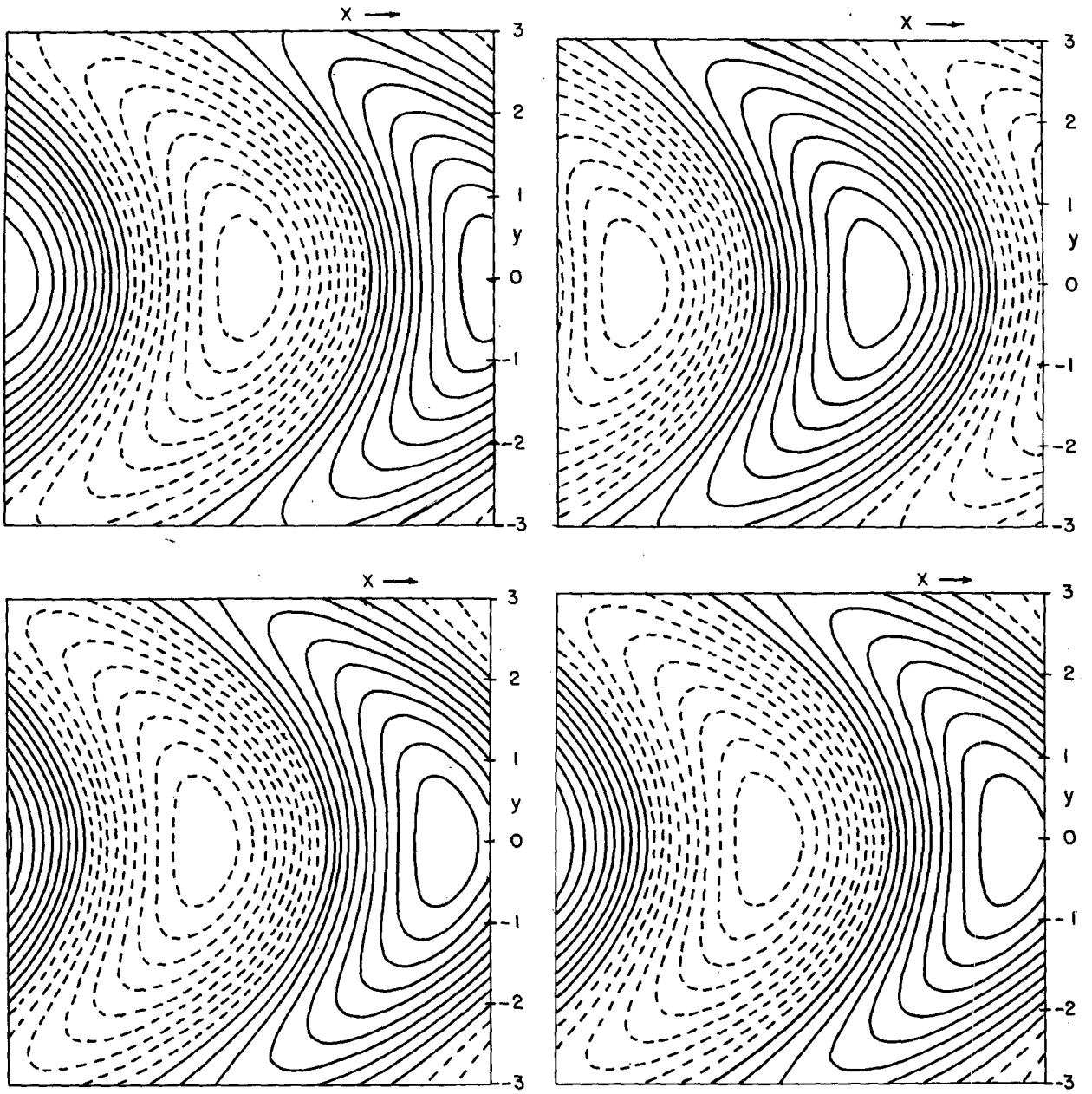

FIG. 2. Horizontal distributions of the dimensionless (a) moist entropy perturbation T, (b) zonal velocity perturbation u, (c) vertical velocity w, and (d) cumulus mass flux, calculated at the top of the mixed layer for wavenumber 1 for the case $F = 0.9$ and $\gamma = 0.2$. Dashed lines denote negative values. For a zonal velocity amplitude of 1, the amplitudes of T, w, and the cumulus mass flux are 1.71, 0.99 and 0.95, respectively. The ordinate is dimensionless meridional distance with one unit representing approximately nine degrees latitude.

cooling, while the part due to evaporation drives the wave.

Figure 2 shows that the negative zonal velocity perturbations lead the θ_e^* perturbations by a little less than 45° and that the cumulus mass flux field strongly resembles the total vertical velocity. The relative amplitudes of the quantities are such that with the normalizations given by (25) together with the parameters listed in Table 1 and $[U^*] = 2$ m s^{-1}, a zonal velocity perturbation of 2 m s^{-1} would be accompanied by a θ_e perturbation of 1.3°C and a vertical velocity amplitude of 0.3 cm s^{-1}. The θ_e fluctuation corresponds to a relative humidity variation of about 1.9%, which is near the noise level of most measurements; this perhaps partially explains the failure of Madden and Julian (1971) to detect any significant correlations between mixing ratio and zonal wind. The meridional structure of the perturbations strongly resembles the wavenumber 1 component of oscillations in outgoing longwave radiation found by Murakami et al. (1986), with pole-

ward phase propagation increasing in magnitude away from the equator.

4. Scale selection

The growth rate of the linear disturbances given by (31) increases as k^2 for small k and $k^{1/2}$ for large k, pointing to a defect in the formulation of the problem. We here argue that this defect is related to the assumption that heat acquired by the boundary layer is immediately redistributed aloft by convection, and that the heat appears only as a strictly local temperature change. In a stratified fluid, however, even a point source of heat results in a temperature change that occurs on the time scale of a pendulum day and is distributed over a volume whose horizontal dimension is the deformation radius. On the equatorial β-plane, Gill (1980) has shown that a maintained point source of heat results in a circulation which is elongated in the zonal direction and extends poleward to a distance on the order of the equatorial deformation radius. Thus, if the meridional scale of the waves in the present model is much shorter than the equatorial deformation radius, the temperature perturbations associated with the waves would in nature be smoothed out over a distance large compared to the wave. We therefore demand, in order that the solutions be viable, that the meridional scale of the wave be comparable to or greater than the equatorial deformation radius. In other words, we ask that that scale of the wave should be comparable to or larger than the scale of convective circulations, where the latter *includes* the subsidence around the convection. From (33) and (31), in the small k limit, together with the normalizations (25), the meridional scale of the disturbances is of order

$$L_y = 2a^{1/2}C_D^{1/2}U^{*1/2}h^{-1/2}k^{-1/2}\beta^{-1/2}.$$

Requiring this to be comparable to or larger than the equatorial deformation radius $(NH/2\beta)^{1/2}$ results in the requirement that

$$k \ll 8C_D a U^* N^{-1} H^{-1} h^{-1} \approx 1.0 U^*,$$

where we have used values of the parameters listed in Table 1 and $NH = 100$ m s^{-1}. Evidently, only the longest waves are comparable in size to the convective circulations which are assumed to redistribute heat upward from the boundary layer.

Another mechanism may select wavenumber 1 at finite amplitude. There will evidently be a limit on the maximum descending motion which can occur in the wave; this is determined by the amount of subsidence warming which can be compensated for by radiational cooling. If the subsidence exceeds this critical rate, warming will occur in the descending air and the wave will be damped. From the thermodynamic equation, the critical subsidence rate is

$$w_{\text{crit}} = \frac{g\dot{Q}}{N^2 C_p T},$$

where $\dot{Q}$ is the radiational heating and N is the buoyancy frequency. For $\dot{Q}/C_p = 1$°C day^{-1} and $N = 10^{-2}$ s^{-1}, this amounts to about 0.4 cm s^{-1}. From the mass continuity equation, u will be limited by

$$|u|_{\text{crit}} = |w_{\text{crit}}|\frac{a}{h'k},$$

where h' is the altitude at which w peaks, a is the earth's radius, and k the zonal wavenumber. Clearly, zonal wavenumber 1 will have the maximum amplitude for a fixed w_{crit}. From the aforementioned value of w_{crit} and $h' = 5$ km, this amounts to about 5 m s^{-1}. While this mechanism selects wavenumber 1 in the zonal velocity perturbations, it does not clearly select $k = 1$ in the vertical velocity field and in related fields such as clouds and precipitation. The modeling experiment of Hayashi and Sumi (1986) does show considerable noise in the precipitation fields, though they are clearly modulated by wavenumber 1.

5. Nongeostrophic modes

The system of equations (27)–(29) also admits a set of nongeostrophic modes for which u and T vanish at the equator. Eliminating u and v from the system results in

$$\frac{dT}{dy} = -T\left[D_3 y + \frac{D_2}{Py}(ik + D_1 D_3)\right], \tag{38}$$

where

$$\left.\begin{aligned} D_1 &\equiv \sigma + ik[U] + 2F \\ D_2 &\equiv \sigma + ik[U] + F \\ D_3 &\equiv \sigma + ik[U] + \gamma \end{aligned}\right\}. \tag{39}$$

The solution of (38) is

$$T = y^{-(D_2/P)(ik+D_1D_3)} \exp\left[\frac{1}{2}D_3 y^2\right]. \tag{40}$$

The requirement that T be well behaved near the equator implies that

$$D_2(ik + D_1 D_3) = -nP, \tag{41}$$

where n is a positive integer. The corresponding solutions for u and v are

$$\left.\begin{aligned} u &= -D_3 y^n \exp\left[-\frac{1}{2}D_3 y^2\right] \\ v &= -(ik + D_1 D_3) y^{n-1} \exp\left[-\frac{1}{2}D_3 y^2\right] \end{aligned}\right\}. \tag{42}$$

Setting $n = 0$ in (41) recovers the modes discussed in section 3. For finite n, the right-hand side of (41) is large, since $P \approx$ O(30). If D_1, D_2 and D_3 are of the same magnitude, this implies that for $k \ll (nP)^{2/3}$, the approximate dispersion relation is

$$D_1 D_2 D_3 = -nP.$$

If the friction and radiative damping terms are negligible compared to σ, the growing solutions are

$$\sigma = (nP)^{1/3}\left[\frac{1}{2} \pm \frac{\sqrt{3}}{2}i\right] - ik[U]. \tag{43}$$

Thus in the case where $k = 0$ the solutions consist of oscillations centered at the equator which, according to (40) and (42), are symmetric in v and antisymmetric in u and T if n is odd, while the converse holds when n is even. Since P is large, these are short period oscillations. Table 2 shows dimensional growth rates, phase speeds and periods of the zonally symmetric ($k = 0$) and wavenumber 1 modes as exact solutions of (41) for the case $n = 1$. All modes listed have periods of around 6 days and westward-traveling modes are seen to exist, but have slightly smaller growth rates than the eastward-propagating waves. The phase speeds of the wavenumber 1 modes are comparable to those of free Kelvin waves. Inspection of (40) shows that the meridional decay scale of the oscillations is

$$L_y \approx \sqrt{2/D_3} \approx 2(nP)^{-1/6}.$$

For $n = 1$, $k = 0$ and typical values of the parameters (those listed in Table 1), this decay scale is about 1000 km, which is somewhat less than the equatorial deformation radius. Thus it is difficult to satisfy the requirement that the circulations be comparable to or larger than the deformation radius. On the other hand, the growth rates can be large. Thus we cannot rule out altogether the possibility of short period oscillations with meridional index (n) of 1 or 2, though these have not as yet been observed.

6. Effects of meridionally varying sea surface temperature

The sea surface temperature (SST) enters the physical system through its effect on the mean air–sea equivalent potential temperature difference. Inspection of (24) shows that this dependence enters the same term as that which multiplies sgn[U]. This is also true of the thermodynamic efficiency, ϵ. Thus we may rewrite (29) as

$$(D+\gamma)T = -uB(y), \tag{44}$$

where we have chosen $\bar{U} < 0$ and $B(y)$ is a dimensionless function of y. For the geostrophic ($n = 0$) modes, (27) and (44) are still decoupled from (28) at the equator, so that the dispersion relation is

$$(D+2F)(D+\gamma) = -ikB(0). \tag{45}$$

This shows that *the growth rate and phase speed depend only on the sea surface temperature and thermodynamic efficiency at the equator.* On the other hand, the meridional structure deduced from (28) will depend on the form of $B(y)$, and v will not vanish everywhere unless $B(y)$ is constant. Since D and v are order 1 quantities, and $P \approx 30$, we make the geostrophic approximation by neglecting the left-hand side of (28). Combining (28) with (44) and using (45) and (27) results in the following equations for the structures of T, u and v:

$$\left.\begin{aligned} T &= \exp\left[-(D+\gamma)\int_0^y \frac{y}{B(y)}\,dy\right] \\ u &= -T(y)\frac{D+\gamma}{B(y)} \\ v &= ikT(y)\frac{B(0)-B(y)}{yB(y)} \end{aligned}\right\}. \tag{46}$$

We also diagnose the (dimensional) vertical velocity w from mass continuity,

$$w = -\frac{dv}{dy} - iku,$$

and use (37) to estimate the cumulus mass flux. As an example of the effect of meridional variations of sea surface temperature or ϵ on the structure of the modes, we calculate the mode structures for the case

$$B(y) = \frac{1}{1+\alpha(y-y_0)^2},$$

where y_0 is the latitude at which the SST peaks and α measures the rate of decay of SST and/or ϵ away from y_0. Figure 3 shows the T, u, v and w fields for $y_0 = 0$ and $\alpha = 1$. (The cumulus mass flux is not shown since it strongly resembles the w field.) This represents a very strongly peaked SST field, with the air–sea equivalent potential difference and/or ϵ falling off to about half its equatorial value at a latitude of about 10°. The θ_e field is somewhat more concentrated around the equator than in the case of uniform SST (see Fig. 2a), and the u and w fields have maxima off the equator. The eddy flux of angular momentum is

TABLE 2. Growth rates, phase speeds, and periods of low-order nongeostrophic modes ($n = 1$)†.

k	$-[U^*]$ (m s^{-1})	σ_r^* (day^{-1})	c^* (m s^{-1})	Period (days)
0	4	−0.01		6.6
	3	0.13		6.3
	2	0.28		6.1
	1	0.45		5.9
1	4	−0.05	−69	6.7
		0.02	+72	6.5
	3	0.10	−72	6.4
		0.17	+75	6.2
	2	0.25	−75	6.2
		0.32	+78	5.9
	1	0.41	−77	6.1
		0.48	+79	5.8

† Using the same parameter values as those listed in Table 1 and $P = 32.7$.

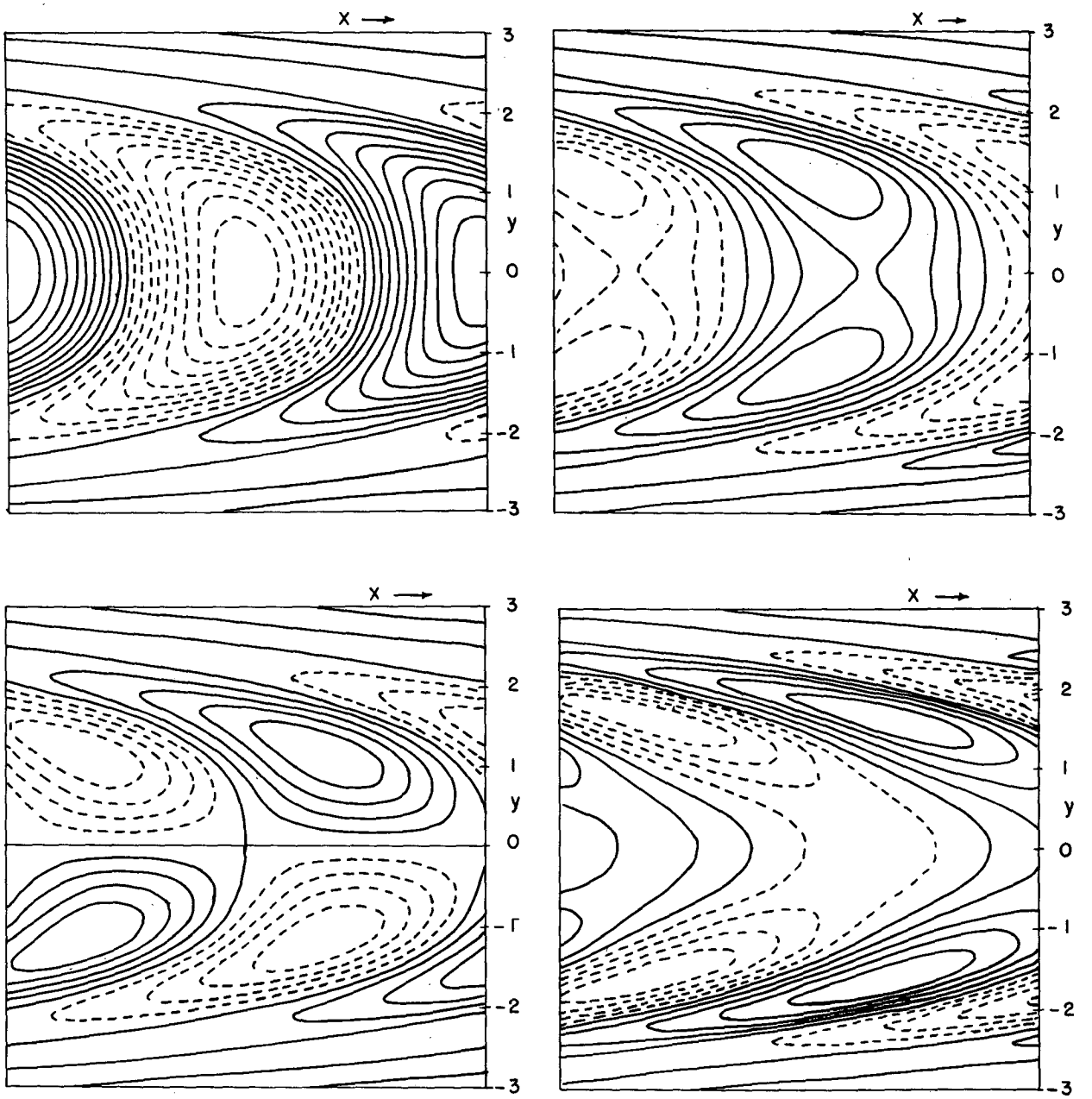

FIG. 3. Horizontal distributions of (a) T, (b) u, (c) v and (d) w as in Fig. 2, but for the quantity A defined by (26) varying according to $A = 1/(1 + y^2)$. For a zonal velocity amplitude of 1 the amplitudes of T, v and w are 1.04, 0.84 and 2.81, respectively.

$$\frac{1}{2}\,\mathrm{Re}[u^* v] = \frac{k^2 c |T|^2}{|D+\gamma|^2}\,\frac{B(0)-B(y)}{2\gamma B^2(y)}, \tag{47}$$

where c is the intrinsic phase speed. This shows that the eddy angular momentum flux is always *away* from the sea surface temperature maximum. Since u and v both change sign across the middle troposphere, this correlation holds in the upper troposphere, as well. It is thus possible that the 30–60 day waves help to sustain equatorial easterlies.

Figure 4 shows various fields for the case that $y_0 = 0.5$ (about 5° latitude) and $\alpha = 0.5$. While the asymmetry in the temperature (pressure) field is barely noticeable, the u, v and w fields peak on the opposite side of the equator from the SST maximum. Since the geostrophic balance condition (28) requires dT/dy to vanish at the equator, stronger winds are necessary south of the equator to achieve the same heat flux as that which occurs north of the equator. Inspection of (47) shows that the angular momentum flux is always away

from the latitude where $B(y) = B(0)$; this contributes to the generation of easterlies poleward of the SST maximum.

7. Effects of zonally varying sea surface temperature

In the earth's atmosphere, the sea surface temperature varies considerably along the equator, as does the air–sea equivalent potential temperature difference. Moreover, part of the equatorial belt is covered by the land areas of South America, Africa, and the maritime continent of the East Indies. The surface θ_e flux over land is highly dependent on incoming solar radiation, even on short time scales, and thus bears little relation to the surface wind speed, although the latter can have a modifying effect. Roughly $\frac{1}{6}$ of the equator is covered by land; thus as a first approximation, the value of $\ln\theta_{es}/\theta_e$ which appears in (24) and in the definition of A (26) should be reduced by $\frac{1}{6}$. This reduces the growth rate and phase speed by 25/36 and 5/6, respectively, in the small k limit, and by $\sqrt{5/6}$ in the large k limit. The fact that the mean water temperature is somewhat lower than the value used in Table 2 should lead to a further reduction in phase speed. These effects may partially explain the tendency for aqua-planet GCM simulations, such as that described by Hayashi and Sumi (1986), to give phase speeds which are somewhat higher than observed.

We here make a crude attempt to account for zonally varying SST by solving the system (27), (29) on the equator with a variable SST. This system may be written

$$\left.\begin{aligned}(D+2F)u &= \frac{\partial T}{\partial x}\\ (D+\gamma)T &= -C(x)u\end{aligned}\right\}, \tag{48}$$

where $D \equiv \sigma + [U](\partial/\partial x)$ and $C(x)$ reflects the zonal variability of the SST. We solve (48) using the function

$$C(x) = 1 + \epsilon \sin x,$$

where ϵ is a small parameter. By expanding u, T and σ in series involving powers of ϵ, it is possible to solve (48) to an arbitrary power of ϵ. The solution to order ϵ for u has the form

$$u = e^{\sigma_r t}[e^{ik(x-ct)}\epsilon C_1(1+k)e^{i(k+1)[x-(kc/k+1)t]} + \epsilon C_2(1-k)e^{i(k-1)[x-(kc/k-1)t]} + O(\epsilon^2)], \tag{49}$$

where C_1 and C_2 are constants. One can see that the wavenumber 1 variation of the SST modulates a wavenumber k disturbance to produce a wavenumber $k+1$ wave traveling at a speed of $ck/(k+1)$ and a wavenumber $k-1$ wave with a phase speed of $ck/(k-1)$. In particular, a wavenumber 1 disturbance excites a wavenumber 2 response with half the phase speed. By eliminating T between (48) and (28) (in the limit of large P), we can form a relation for the meridional structure of u:

$$\left(\sigma + 2F + [U]\frac{\partial}{\partial x}\right)yu = -C(x)\frac{du}{dy}. \tag{50}$$

Inspection of (50) and (49) shows that the exponential decay scale is governed principally by $\sigma_r + 2F$ and thus is approximately the same for all the waves, to order ϵ. This may indicate that the wavenumber 2 which results from the modulation of wavenumber 1 by zonally varying SST is more likely to occur in nature than the directly unstable wavenumber 2, since the latter decays more rapidly with y.

8. Effects of meridionally varying mean zonal wind

The zonal mean zonal winds in the atmosphere vary considerably over the range of latitudes in which the 30–60 day wave has detectable amplitude, showing a tendency to exhibit a peak easterly component at or near the equator. Examination of (16), (17) and (24) shows that variable mean winds affect the damping and zonal advection terms, while the wind-dependent heat term depends only on the sign of $[U]$. Also, meridionally varying $[U]$ introduces a meridional advection term into (16). To be consistent, we must suppose that the meridional variability of $[U]$ is purely barotropic; otherwise it is necessary to introduce a mean meridional θ_e gradient as well.

We have seen (in section 3) that meridionally bounded solutions are only possible when $[U] < 0$. We shall therefore be restricted to profiles of $[U]$ which satisfy $[U] < 0$ everywhere within the belt in which the solutions have appreciable amplitude. With this restriction, (27)–(29) take the form

$$(\sigma + ik[U] + 2F'|[U]|)u = ikT + v(y - [U]_y), \tag{51}$$

$$\frac{dT}{dy} = yu, \tag{52}$$

$$(\sigma + ik[U] + G'|[U]| + \gamma)T = -u, \tag{53}$$

where we have made the geostrophic approximation ($P \gg 1$), and

$$F' \equiv C_D a h^{-1}, \quad G' \equiv C_\theta a H^{-1}.$$

It is once again seen that for modes for which u and T are finite at the equator, (51) and (53) are decoupled from (52) provided $[U]_y = 0$ at $y = 0$. *The dispersion relation, then, depends only on the zonal wind at the equator.* The meridional structure of the various fields depends, however, on the structure of $[U](y)$. The variation of u and T with y can be found from (52) and

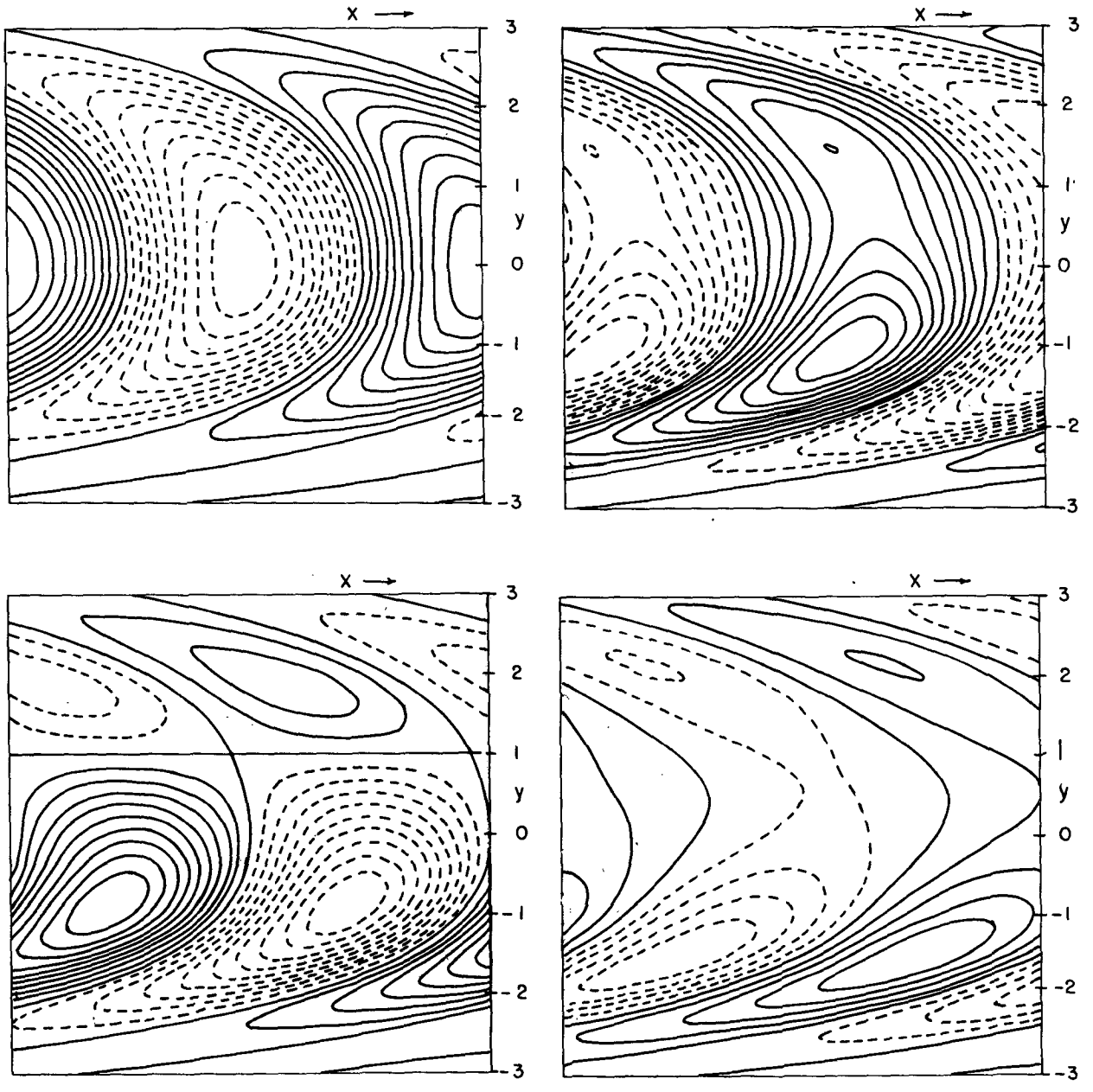

FIG. 4. As in Fig. 3, but for A varying according to $A = 1/[1 + 0.5(y - 0.5)^2]$. For a zonal velocity amplitude of 1 the amplitudes of T, v and w are 1.13, 0.79, and 2.19, respectively.

(53), while v may be diagnosed using (51). The results are

$$T = \exp\left[-\tfrac{1}{2}(\sigma+\gamma)y^2 - (ik - G')\int_0^y y[U]dy\right],$$

$$u = -T(\sigma + \gamma + (ik - G')[U]),$$

$$v = T \times \langle [\sigma(2ik - 2F' - G') + \gamma(ik - 2F')]([U](0) - [U](y)) + (ik - 2F')(ik - G')([U]^2(0) - [U]^2(y))\rangle/(y - [U]_y)$$

The vertical velocity and cumulus mass flux can then be deduced from the mass continuity equation and (37).

Figure 5 presents the various fields for the case that

$$[U] = \frac{-0.05}{1 + y^2}.$$

For this calculation, we have taken $\gamma = 0$, $F' = 12$ and $G' = 1$. The u and T fields decay slightly less rapidly with latitude since the effective damping terms fall off

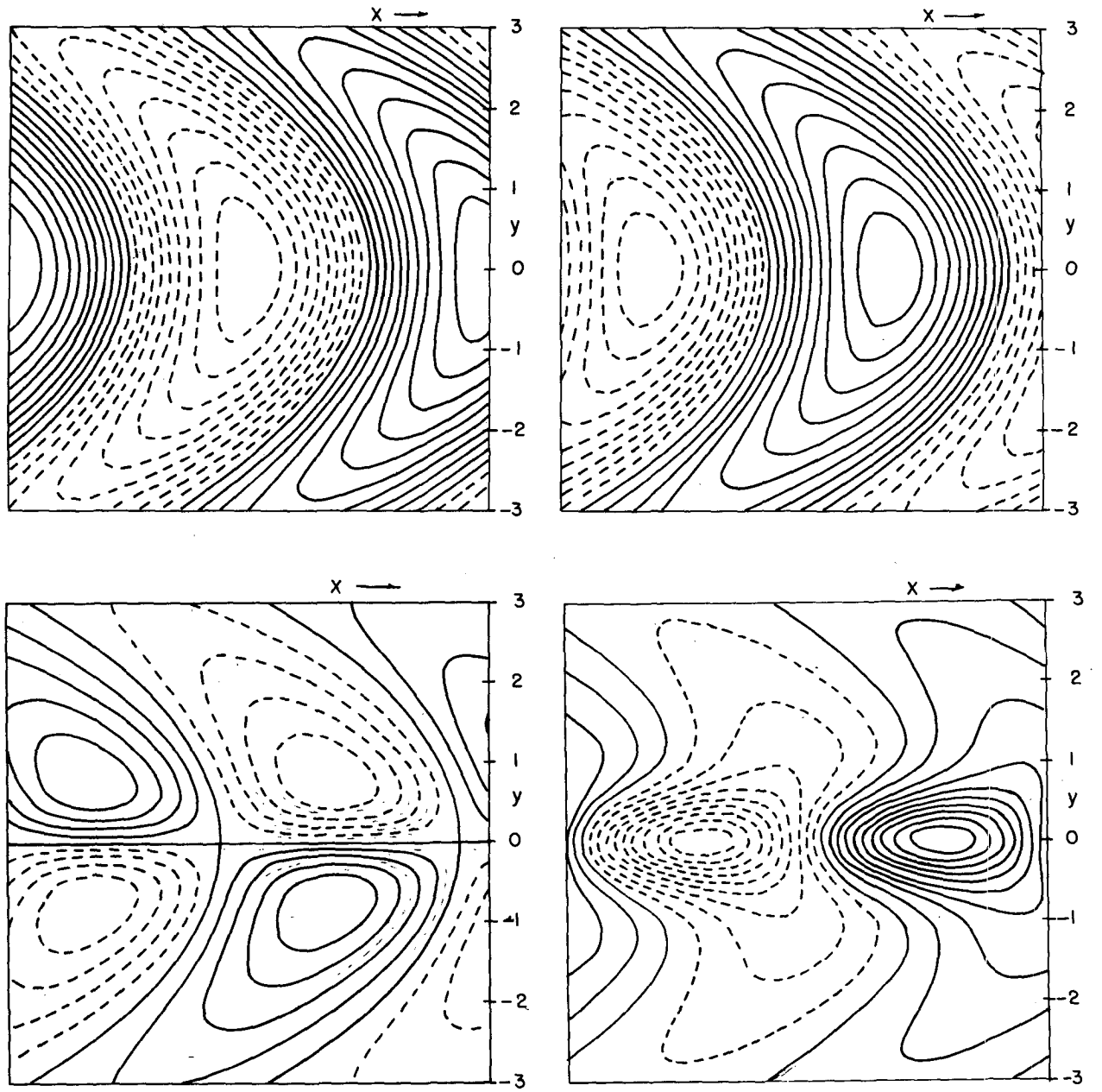

FIG. 5. Horizontal distributions of (a) T, (b) u, (c) v and (d) w for $\gamma = 0$, $F' = 12$, and $G' = 1$ for mean zonal wind varying according to $[U] = -0.05/(1 + y^2)$. For a zonal velocity amplitude of 1.0 the amplitudes of T, v, and w are 1.53, 0.62 and 1.83, respectively.

with latitude. Vertical velocity and cumulus mass flux (the latter is not shown but is nearly identical to w) are strongly concentrated at the equator. Inspection of the u and v fields shows that in this case the eddy angular momentum flux is toward the equator. The eddies thus act to smooth out the initial negative maxima of $[U]$ at the equator.

The T, u, v and w fields are shown in Fig. 6 for the case that

$$[U] = 0.25 \cos \pi y - 0.075,$$

giving local *maxima* of $[U]$ of -0.05 at the equator and at $y = \pm 2, \pm 4$ etc.; with local minima of -0.1 at $y = \pm 1, \pm 3 \cdots$. The vertical velocity and cumulus mass flux (not shown) show peaks at the equator and at $y \approx \pm 1$, and in this case the eddy angular momentum flux is poleward, reaching a peak magnitude at about $y = \pm 0.7$. This acts to accelerate the easterly flow near the equator and diminish it near the existing peaks at $y = \pm 1$. Since the climatological surface wind field shows peak easterlies on either side of the equator (e.g.,

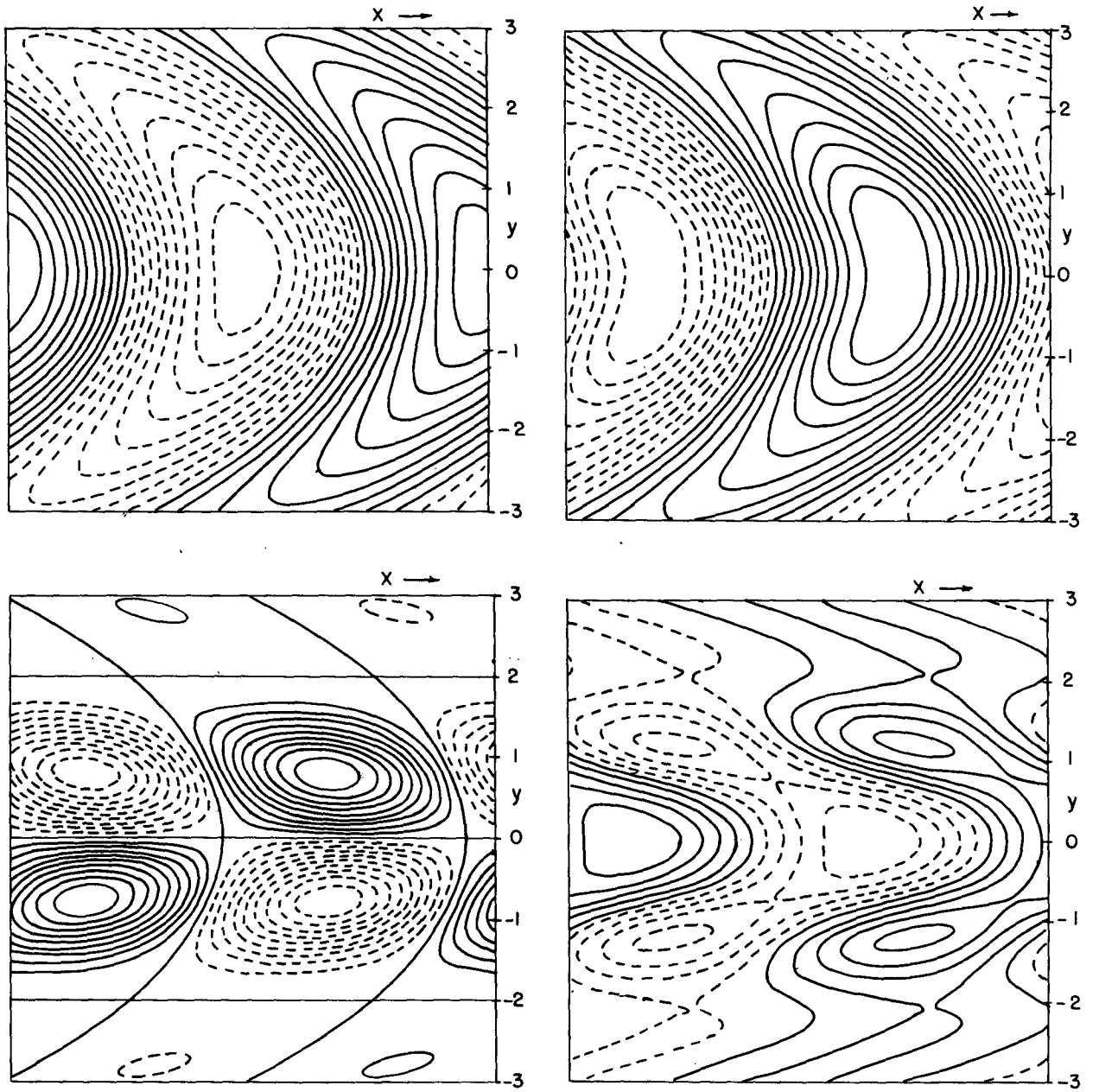

FIG. 6. As in Fig. 5 but for $[U] = 0.025 \cos\pi y - 0.075$. For a zonal velocity amplitude of 1.0, the amplitudes of T, v and w are 1.51, 1.42 and 2.80, respectively.

see Newell, 1972) the 30–50 day waves may act to sustain easterlies at the equator.

9. Conclusions

The simple theory for the 30–60 day oscillation presented here is based on the idea that the oscillation is a manifestation of an air–sea interaction instability drived by wind-dependent surface fluxes of moist entropy. Moist convection is assumed to immediately redistribute aloft the heat acquired from the sea and does not act as a heat source in and of itself. (Latent heat release due solely to moisture convergence, unaccompanied by surface fluxes, exactly balances adiabatic cooling.) The basic mechanism is described heuristically in Fig. 1: Anomalous surface heat fluxes occur in the easterly phase of the wave, giving rise to temperature perturbations which lead the surface convergence by about ¼ cycle. This increases the amplitude of the wave, as temperature is positively correlated with ver-

tical velocity, and leads to eastward propagation. A simple linear model based on this idea, presented in section 3, gives reasonable phase speeds and periods for wavenumber 1, but implies that shorter waves should dominate the spectrum. In section 4 we argue that the selection of wavenumber 1 may be due to the tendency for gravity waves to distribute temperature perturbations over a meridional distance proportional to the equatorial deformation radius and to the tendency for the waves to saturate when the downward vertical velocity of the waves is such that subsidence warming can no longer be balanced by radiational cooling.

While the zonal wavenumber 1 disturbance has zonal velocity perturbations which are very nearly in geostrophic balance, the linear model also admits various nongeostrophic modes for which the zonal velocity, temperature and pressure perturbations vanish at the equator. Among these are various zonally symmetric modes. The nongeostrophic modes are considerably faster, with periods on the order of a week.

The meridional structure of the geostrophic disturbances is affected by meridional variations in the thermodynamic efficiency (ϵ), the sea surface temperature and the mean zonal wind. The growth rates and phase speeds, however, depend only on conditions right at the equator. The eddy angular momentum fluxes tend to be toward regions of maximum mean low-level easterly flow and away from latitudes with the highest sea surface temperatures and thermodynamic efficiencies. The tendency to carry angular momentum away from sea surface temperature maxima and toward maxima in the surface easterlies may help explain the maintenance of easterlies at the equator.

While the linear model tends to support the heuristic description outlined in the Introduction and illustrated in Fig. 1, it does not adequately explain the observed preference for low wavenumbers, and it is inherently incapable of predicting the amplitude of the waves. The model does, however, make certain predictions which can easily be tested in the context of general circulation models. The most obvious of these is the prediction that the intrinsic phase speed of the disturbances should vary with the surface exchange coefficient, the temperature difference across the depth of the troposphere, the inverse of the pressure depth of the troposphere, and the air–sea equivalent potential temperature difference; all evaluated at the equator [see Eqs. (31) and (26)]. This test should provide a relatively straightforward confirmation or refutation of the hypothesis advanced in this paper.

Acknowledgments. This work was supported by the National Science Foundation under Grant ATM-8513871. The author thanks Laura Doughty for typing the manuscript and Isabelle Kole for drafting the figures.

APPENDIX

Relationships between Changes in Mean Tropospheric Temperature, Moist Entropy and Precipitation Rate

In section 2 we postulate that fluctuations in the saturated moist entropy of the troposphere (s^*) are proportional to fluctuations in the pressure-weighted average moist entropy $\bar{s}$:

$$\delta s^* = \nu \delta \bar{s}. \tag{A1}$$

Here we show that ν may be related alternatively to the degree of moistening of the environment by clouds or to the fraction of anomalous evaporation that is manifested in anomalous rainfall.

From the definition of θ_e, the equivalent potential temperature, we may write

$$s = C_p \ln\theta_e = C_p \ln\theta + \mathrm{RH}\frac{Lq_s}{T_c}, \tag{A2}$$

where θ is the potential temperature, RH is the relative humidity, L the heat of vaporization, C_p the heat capacity at constant pressure, q_s the saturation mixing ratio and T_c the condensation temperature. The above may alternatively be expressed

$$s = \mathrm{RH}\frac{T}{T_c}s^* + \left(1 - \mathrm{RH}\frac{T}{T_c}\right)s_d, \tag{A3}$$

where s^* and s_d are the saturation moist entropy and dry entropy, respectively. From (A3), fluctuations in s may be expressed

$$\delta s = \left[\frac{\Gamma_m}{\Gamma_d} + \mathrm{RH}\frac{T}{T_c}\left(1 - \frac{\Gamma_m}{\Gamma_d}\right)\right]\delta s^* + (s^* - s_d)\delta\left(\mathrm{RH}\frac{T}{T_c}\right), \tag{A4}$$

where we have made use of the relation

$$\delta s_d = \frac{\Gamma_m}{\Gamma_d}\delta s^*, \tag{A5}$$

and Γ_m and Γ_d are the moist and dry adiabatic lapse rates, respectively. If we assume that the temperature lapse rate is always moist adiabatic then fluctuations in s^* will be constant with height, so that averaging (A4) through the depth of the troposphere results in

$$\delta s^* = \frac{1}{\chi}\overline{\left[\delta\bar{s} - (s^* - s_d)\delta\left(\mathrm{RH}\frac{T}{T_c}\right)\right]}, \tag{A6}$$

where

$$\chi \equiv \frac{\Gamma_m}{\Gamma_d} + \mathrm{RH}\frac{T}{T_c}\left(1 - \frac{\Gamma_m}{\Gamma_d}\right), \tag{A7}$$

and the overbar denotes an average in pressure from cloud base to the tropopause:

$$(\bar{\ }) = \frac{1}{p_b - p_t}\int_{p_t}^{p_b} (\ )\,dp,$$

where p_b and p_t are the pressures at the top of the boundary layer and tropopause, respectively.

The quantity χ defined by (A7) has a minimum value of about 0.5 at high temperature and very low relative humidity, and a maximum value of 1 when the air is saturated. If the relative humidity is everywhere about 0.5, then $\bar{\chi}$ is about 0.8 in the tropics. Equation (A6) informs us that if fluctuations in $\bar{s}$ are not accompanied by humidity fluctuations, then δs^* is slightly greater than $\delta\bar{s}$. If, however, the fluctuations of $\bar{s}$ are associated with substantial fluctuations of mean relative humidity, then δs^* is less than $\delta\bar{s}$.

The proportionality constant ν that appears in (A1) may also be related to the precipitation rate. Neglecting radiation, the thermodynamic equation may be written

$$C_p\left(\rho\frac{\partial T}{\partial t} + \nabla\cdot\rho\mathbf{V}T\right) - \omega = -L\left(\rho\frac{\partial q}{\partial t} + \nabla\cdot\rho\mathbf{V}T\right), \quad \text{(A8)}$$

where ρ is the density and ω is the time rate of change of pressure. If (A8) is averaged over a volume the depth of the troposphere and large enough that velocity perturbations associated with convection vanish at the boundaries (i.e., with dimensions of the deformation radius) we obtain

$$C_p\left[\rho\frac{\partial T}{\partial t}\right] = -L\left[\rho\frac{\partial q}{\partial t}\right], \quad \text{(A9)}$$

where the brackets denote the volume average and we have noted that $[\omega] = 0$. If we further assume that horizontal variations of ρ are negligible in (A9), the latter may be written

$$C_p\int_0^{H_T}\rho\frac{\partial T}{\partial t}dz = -L\int_0^{H_T}\rho\frac{\partial q}{\partial t}dz = LP_0, \quad \text{(A10)}$$

where P_0 is the surface precipitation rate and T and q are assumed to be averages over the horizontal area of the aforementioned volume. Using the hydrostatic equation and (A5) the left-hand side of (A10) can be expressed

$$C_p\int_0^{H_T}\rho\frac{\partial T}{\partial t}dz = \frac{C_p}{g}\int_{p_t}^{p_b}\frac{\partial T}{\partial t}dp = \frac{1}{g}\int_{p_t}^{p_b}T\frac{\partial s_d}{\partial t}dp$$
$$= \frac{1}{g}\int_{p_t}^{p_b}T\frac{\Gamma_m}{\Gamma_d}\frac{\partial s^*}{\partial t}dp. \quad \text{(A11)}$$

Using the definitions of Γ_m and Γ_d and the hydrostatic equation, (A11) may alternatively be written

$$C_p\int_0^{H_t}\rho\frac{\partial T}{\partial t}dz = \frac{1}{g}\frac{C_p}{R}\frac{\partial s^*}{\partial t}\int_{p_t}^{p_b}p\left(\frac{\partial T}{\partial p}\right)_{s^*}dp, \quad \text{(A12)}$$

where we have made use of the invariance of $\partial s^*/\partial t$ with height. Using this in (A10) and integrating by parts we get

$$\epsilon_2\frac{\partial s^*}{\partial t} = \frac{R}{C_p}\frac{L}{T_b}\frac{g}{\Delta p}P_0, \quad \text{(A13)}$$

in which

$$\epsilon_2 \equiv \frac{p_bT_b - p_tT_t}{T_b\Delta p} - \frac{\bar{T}}{T_b}. \quad \text{(A14)}$$

Finally, we assume that precipitation anomalies are a fixed fraction of surface evaporation anomalies and write (A13) as

$$\epsilon_2\frac{\partial s^*}{\partial t} = \epsilon_p\frac{R}{C_p}\frac{L}{T_b}\frac{E_0}{H} = \epsilon_p\frac{R}{C_p}\frac{\partial\bar{s}}{\partial t}, \quad \text{(A15)}$$

where ϵ_p is the fraction of anomalous surface evaporation realized as anomalous precipitation and E_0 is the surface evaporation rate. Comparing (A15) with (A1) it is evident that

$$\nu = \frac{\epsilon_p}{\epsilon_2}\frac{R}{C_p}. \quad \text{(A16)}$$

Estimates of ϵ_2 in the tropics yield values around 0.16, so that

$$\nu \approx 1.8\epsilon_p.$$

Comparing this with (A6) it is seen that the efficiency ϵ_p must be less than about $\frac{2}{3}$ unless tropospheric relative humidity fluctuations are negatively correlated with fluctuations in $\bar{s}$, which seems highly unlikely.

These arguments, taken together, suggest that ν is close to unity in regions of the atmosphere in which precipitation is active and small otherwise. From the standpoint of the present linear model, we will assume that the oscillation occurs in an atmosphere in which precipitation is occurring in the mean state, so that anomalous evaporation leads to anomalous precipitation. This accords well with observations which show that the wave is active principally in the high precipitation regions of the western equatorial Pacific and Indian Oceans, and also is consistent with the mean precipitation distribution in simulations such as those of Hayashi and Sumi (1986). In the calculations presented in the text we take $\nu = 0.8$.

REFERENCES

Anderson, J. R., and R. D. Rosen, 1983: The latitude–height structure of 40–50 day variations in atmospheric angular momentum. *J. Atmos. Sci.*, **40**, 1584–1591.

Betts, A. K., 1982: Saturation point analysis of moist convective overturning. *J. Atmos. Sci.*, **39**, 1484–1505.

Cane, M., 1983: Oceanographic events during El Niño. *Science*, **222**, 1189–1195.

Chang, C.-P., 1977: Viscous internal gravity waves and low frequency oscillations in the tropics. *J. Atmos. Sci.*, **34**, 901–910.

Deardorff, J. W., 1972: Parameterization of the planetary boundary layer for use in general circulation models. *Mon. Wea. Rev.*, **100**, 93–106.

Emanuel, K. A., 1986: An air–sea interaction theory for tropical cyclones. Part I: Steady state maintenance. *J. Atmos. Sci.*, **43**, 585–604.

Gill, A. E., 1980: Some simple solutions for heat-induced tropical circulation. *Quart. J. Roy. Met. Soc.*, **106,** 447–462.

Goswami, B. N., and J. Shukla, 1984: Quasi-periodic oscillations in a symmetric general circulation model. *J. Atmos. Sci.*, **41,** 20–37.

Hayashi, Y., 1970: A theory of large-scale equatorial waves generated by condensation heat and accelerating the zonal wind. *J. Met. Soc. Japan,* **48,** 140–160.

Hayashi, Y. Y., and A. Sumi, 1986: The 30–40 day oscillations simulated in an "aqua planet" model. *J. Met. Soc. Japan,* **64,** 451–467.

Jordan, C. L., 1958: Mean soundings for the West Indies area. *J. Meteor.,* **15,** 91–97.

Krishnamurti, T. N., P. K. Jayakumar, J. Sheng, N. Surgi and A. Kumar, 1985: Divergent circulations on the 30–50 day time scale. *J. Atmos. Sci.,* **42,** 364–375.

Kuo, H.-L., 1974: Further studies of the influence of cumulus convection on large-scale flow. *J. Atmos. Sci.,* **31,** 1232–1240.

Langely, R. B., R. W. King, I. I. Shapiro, R. D. Rosen and D. A. Salstein, 1981: Atmospheric angular momentum and the length of day: A common fluctuation with a period near 50 days. *Nature,* **294,** 730–732.

Lau, K.-M., and P. H. Chan, 1983a: Short-term climate variability and atmospheric teleconnections from satellite-observed outgoing longwave radiation, Part I: Simultaneous relationships. *J. Atmos. Sci.,* **40,** 2735–2750.

——, and ——, 1983b: Short-term climate variability and atmospheric teleconnections from satellite-observed outgoing longwave radiation, Part II: Lagged correlations. *J. Atmos. Sci.,* **40,** 2751–2767.

——, and ——, 1985: Aspects of the 40–50 day oscillation during northern winter as inferred from outgoing longwave radiation. *Mon. Wea. Rev.,* **113,** 1889–1909.

——, and ——, 1986: The 40–50 day oscillation and the El Niño/Southern Oscillation: A new perspective. *Bull. Amer. Met. Soc.,* **67,** 533–534.

Lindzen, R. S., 1974: Wave-CISK in the tropics. *J. Atmos. Sci.,* **31,** 156–179.

Lorenc, A. C., 1984: The evolution of planetary scale 200 mb divergences during the FGGE year. *Quart. J. Roy. Met. Soc.,* **110,** 427–442.

Madden, R., and P. R. Julian, 1971: Detection of a 40–50 day oscillation in the zonal wind in the tropical Pacific. *J. Atmos. Sci.,* **28,** 702–708.

——, and ——, 1972: Description of global scale circulation cells in the tropics with a 40–50 day period. *J. Atmos. Sci.,* **29,** 1109–1123.

McCreary, J. P., and D. L. T. Anderson, 1984: A model of El Niño and the Southern Oscillation. *Mon. Wea. Rev.,* **112,** 934–946.

Murakami, T., L.-X. Chen, A. Xie and M. L. Shrestha, 1986: Eastward propagation of 30–60 day perturbations as revealed from outgoing longwave radiation data. *J. Atmos. Sci.,* **43,** 961–971.

Neelin, J. D., I. M. Held and K. H. Cook, 1987: Evaporation-wind feedback and low frequency variability in the tropical atmosphere. *J. Atmos. Sci.,* **44,** 2241–2248.

Newell, R. E., J. W. Kidson, P. G. Vincent and G. J. Boer, 1972: *The General Circulation of the Tropical Atmosphere.* Vol. 1, MIT Press.

Parker, D. E., 1973: Equatorial Kelvin waves at 100 millibars. *Quart. J. Roy. Met. Soc.,* **99,** 116–129.

Rosen, R. D., and P. A. Salstein, 1983: Variations in atmospheric angular momentum on global and regional scales and the length of day. *J. Geophys. Res.,* **88,** 5451–5470.

Stevens, D. E., and G. H. White, 1979: Comments on "Viscous internal gravity waves and low-frequency oscillations in the tropics." *J. Atmos. Sci.,* **36,** 545–546.

Webster, P. J., 1983: Mechanisms of monsoon low-frequency variability: Surface hydrological effects. *J. Atmos. Sci.,* **40,** 2110–2124.

Weickmann, K. M., 1983: Intraseasonal circulation and outgoing longwave radiation modes during northern hemisphere winter. *Mon. Wea. Rev.,* **111,** 1838–1858.

——, G. R. Lussky and J. E. Kutzbach, 1985: Intraseasonal (30–60 day) fluctuations of outgoing longwave radiation and 250 mb streamfunction during northern winter. *Mon. Wea. Rev.,* **112,** 941–961.